Spherical Capsule Heating in High Enthalpy Carbon Dioxide in LENS-XX Expansion Tunnel

Matthew MacLean[1]
Aaron Dufrene[2]
Michael Holden[3]
Calspan-University at Buffalo Research Center, Buffalo, NY, 14225

A unique set of experimental measurements have been made in the LENS-XX expansion tunnel facility of the flow over a 17.8-cm spherical capsule heat shield with high enthalpy carbon dioxide test gas traveling from 3.9 to 6.4 km/s (7.6 to 23.5 MJ/kg total enthalpy). Shock shape, surface pressure, and surface heat transfer were measured during six runs and compared to computational fluid dynamics simulations. Unlike previous measurements in the LENS-I reflected shock tunnel facility, the shock shape for all run conditions was found to agree well with the prediction of shock shape and the laminar surface heat transfer distributions were found to lie midway between the predicted non-catalytic and super-catalytic heating bounds predicted, suggesting diffusion-limited finite rate catalytic behavior. The experimental dataset obtained in this study will become a pivotal set of data for validation of thermal and chemical models of Martian entry under realistic conditions.

Nomenclature

C	mass fraction
D	model diameter [cm]
Δh_0	total enthalpy increase over initial total enthalpy [MJ/kg] (Eqn. (3))
h_0	total enthalpy, including chemical formation enthalpy [MJ/kg]
M	Mach number
Re	unit Reynolds number
P	pressure [kPa]
R	model radius [cm]
S	shock standoff distance [cm]
St	Stanton number
T	temperature [K]
U	velocity [km/s]
X	mole fraction
y	radial coordinate [cm]
γ	catalytic reaction efficiency (reactant loss efficiency)
ρ	density [g/m^3]

I. Introduction

SUCCESFUL Entry, Descent, and Landing (EDL) on Mars requires improved knowledge of the complex chemical and thermodynamic kinetics of carbon dioxide. The vibrational reactivity, chemical energy storage, and radiative emission of the constituents of the Martian atmosphere heavily impact the heat shield design[1] necessary for future, large-scale landing missions to explore the Martian surface[2]. Unlike design of hypersonic vehicles for Terran missions, there are exceptionally few opportunities to obtain flight data on Mars, so any data that can be obtained in realistic carbon dioxide environments is critical to the success of the Mars EDL community. The Mars Science Laboratory (MSL) Entry Descent and Landing Instrument (MEDLI) project[3] has provided more flight

[1] Senior Research Scientist; AIAA Senior Member; maclean@cubrc.org.
[2] Research Scientist; AIAA Member.
[3] Vice President of Hypersonics; AIAA Fellow.

data on a Mars flight heat shield than has ever been available before. However, in addition to this data, flight-relevant ground test data in a repeatable, controlled environment is needed. A recent survey of the available ground test data in high enthalpy, reacting carbon dioxide laminar flow by Hollis and Prabhu[4] showed a number of discrepancies and uncertainties in the experiments associated with freestream condition specification, catalytic behavior and interpretation of the data. This survey could not identify any existing run from any ground test facility in which reliable information about laminar, aeroheating in flight relevant enthalpy carbon dioxide could be obtained.

A short test series has been conducted in the LENS-XX facility – a new, large-scale expansion tunnel facility – to assess its viability to fill in the ground testing gap for reacting carbon dioxide environments. These tests have been conducted using an existing spherical capsule model[5] with the intent of comparing the measured shock shape and surface data to CFD simulations for reacting CO_2 test cases. Six runs have been conducted with the model at angle of attack between 18^O and 20^O covering a range of effective total enthalpy between 7.6 and 23.5 MJ/kg (freestream velocity from 3.9 to 6.5 km/s). In all cases, Schlieren images of the shock profile, surface pressure distribution, and laminar surface heat transfer distributions were obtained with the test model.

II. Background of Experimental Facilities and Numerical Tools

A. Experimental Facilities

Currently, CUBRC operates the 48" reflected shock tunnel, the LENS-I and LENS-II reflected shock tunnels[6], and the LENS-XX expansion tunnel[7]. The reflected shock tunnel uses moving shocks to heat and pressurize a stagnant test gas to high enthalpy levels. This test gas may then be expanded through a converging-diverging nozzle in a manner similar to a blowdown facility to produce a hypervelocity test flow. Expansion tunnels like LENS-XX also operate as short duration facilities, but an expansion tunnel produces a high enthalpy flow without the need to first stagnate the test gas. In an expansion tunnel, the bulk of the test gas energy is added through an unsteady expansion in the acceleration segment of the tunnel to produce a low static temperature, high velocity test gas at a thermodynamic state like that of a flight condition. While the useable test times from an expansion tunnel are generally shorter than those from a reflected shock tunnel, the clean, very high enthalpy flows that an expansion tunnel can generate provides a unique testing capability. A notional range of velocity and altitude duplication capabilities for the LENS-XX facility is given for carbon dioxide test gas in Fig. 1. Several relevant trajectories of past Mars missions are shown for reference, scaled assuming a 25-cm scaled model. The horizontal axis of this figure shows the duplicated freestream flight velocity of the entry.

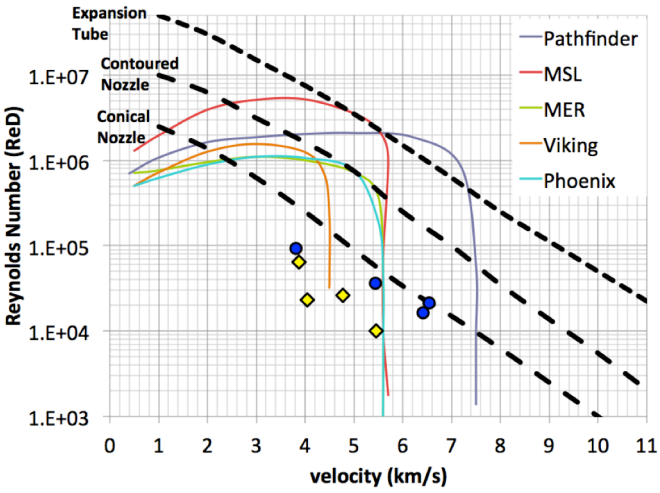

Figure 1. Capability Map of CUBRC LENS-XX Facilities to Test High Enthalpy Carbon Dioxide

B. LENS-XX Operational Overview

The LENS-XX expansion tunnel facility generates test flows in a manner that is very different from the reflected shock tunnel facilities. Reflected shock tunnels operate by driving strong incident and reflected shocks through the test gas which results in a high pressure, high temperature, stagnant reservoir which can be expanded through a converging-diverging nozzle like a blowdown facility. Expansion tunnels do not stagnate the test gas at any time before it flows over the test article. Instead, the test gas is set into motion by a single shock of only weak to moderate strength, and the bulk of the enthalpy in the flow is added as kinetic energy directly by using an unsteady acceleration to increase the velocity. A wave diagram of the basic states of the expansion tunnel is given in Fig 2. In this figure, position is plotted schematically along the horizontal axis and time is plotted qualitatively along the vertical axis. The three test chambers are filled to different pressures and initially separated by diaphragms, where the primary diaphragm between the driver and test gas sections is broken at a time designated as zero. The waves in the diagram are shocks (red), contact surfaces (dotted green) or isentropic expansion fans (blue), where the

thermodynamic state and/or composition of the gases change across any of the waves. Important thermodynamic states of the gases are numbered and the label is colored by the gas composition.

The driver gas (State 4) is a very high pressure, heated, low molecular weight gas (typically hydrogen or helium) that causes a primary shock of moderate strength to move through the test gas when the primary diaphragm is broken. This shock raises the pressure in the test gas just sufficiently to break the secondary diaphragm and causes an initial velocity toward the right in the schematic (State 2). The peak temperature of the test gas during the entire excitation process occurs at State 2, which is typically an order of magnitude lower than a comparable freestream condition in a reflected shock tunnel. For most conditions where it is possible, the State 2 temperature is kept below the threshold where significant chemical dissociation occurs. The moving test gas then accelerates into a much lower pressure acceleration segment (State 10) by unsteady expansion. This causes the test gas to cool and accelerate to very high velocities (State 5). This is the freestream state of the test gas at the end of the tube where tests can be performed in the 0.6-m tube, which can also be expanded through a diverging nozzle into the much larger 2.5-m test section. The freestream velocity obtained is primarily dependent on the molecular weight of the driver gas, the pressure of the driver gas, and the vacuum level of the acceleration segment. Test time available for testing begins at the contact surface between States 20 and 5 and lasts until either the tail of the left-running expansion between States 2 and 5 reaches the test station or until the reflected head of the same wave reaches the test station[8]. The freestream state of the gas typically has a translational temperature near room temperature with a very high velocity. The relative strengths of the primary shock (P_2/P_1) and the unsteady expansion (P_2/P_5) can be utilized to generate different Mach numbers and test conditions for a given total pressure ratio (P_4/P_{10}) which provides a significant degree of flexibility for the facility. Additional details about the LENS-XX facility may be found in the work of Dufrene, et al.[9-10]

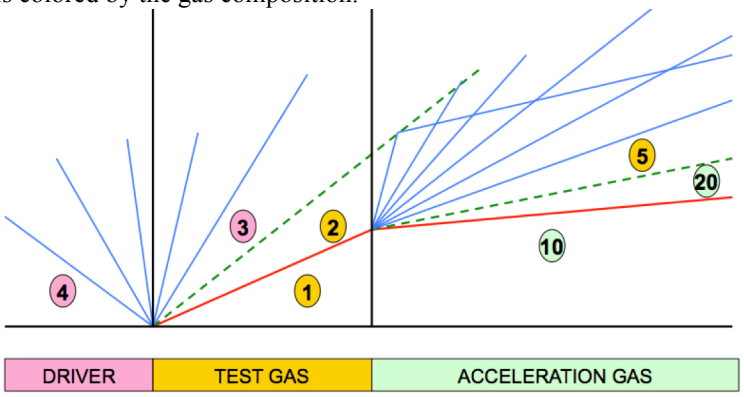

Figure 2. Wave Diagram of an Expansion Tunnel

Determination of test conditions for this facility uses the CHEETAh code discussed by MacLean, et al.[11] This code solves for the intermediate states of the primary and secondary wave systems shown in Fig 2 incorporating equilibrium chemistry, ionization, and thermodynamic excitation mechanisms. This tool provides a simple and accurate way to determine the State 5 condition using measured data from the facility for each run. Single– and Multi– dimensional unsteady simulations of the expansion tube have been performed, but describing the turbulent boundary layer growth in the acceleration tube is a major uncertainty in such calculations. We have found that measuring the Pitot pressure immediately next to the test article provides an additional anchor for the CHEETAh code to most accurately determine the freestream state of the gas. Given the newness of the facility, we cannot yet hope to quantify the uncertainty of the freestream condition specification, but measurements of the freestream velocity using tunable laser diode absorption spectroscopy Doppler shift for selected runs with air test gases[12] were found to agree with the prediction to within the accuracy of the measurement (< 3%).

C. Numerical Tools

The primary, production CFD tool used for LENS facility design, design-of-experiment, and data validation is the Data-Parallel Line-Relaxation (DPLR) code licensed by NASA Ames Research Center (ARC). DPLR is a multi-block, structured, finite-volume code that solves the reacting Navier-Stokes equations including finite rate chemical and thermal non-equilibrium effects. This code is based on the data-parallel line relaxation method[13] and implements a modified (low dissipation) Steger-Warming flux splitting approach[14] for the convection terms and central differencing for the diffusion terms.

Transport properties for the reacting mixtures are modeled in DPLR for high enthalpy flow[15,16] using the binary collision-integral based mixing rules from Gupta, et al[17] with a database of relevant collision integral data for high temperature collisions[18-19]. Diffusion coefficients are modeled using the self-consistent effective binary diffusion (SCEBD)[20].

The DPLR codes allows an arbitrary set of chemical species and reactions to be used; in this work, a standard five-species carbon dioxide model (CO_2, CO, O_2, C, O) was employed for all models using the set of reaction rates published by Park, et al.[21] Reverse reaction rates were computed from equilibrium. Finite rate vibrational

relaxation is modeled via a simple harmonic oscillator vibrational degree of freedom[22] using the Landau-Teller model[23]. Vibrational energy relaxation rates are computed by default from the semi-empirical expression due to Millikan and White[24], but rates from the work of Camac[25] and Park, et al.[21] are substituted for specific collisions where experimental data exists. Vibration-dissociation coupling is currently modeled using the *T-Tv* approach of Park[26].

The DPLR code has several options available to model surface catalysis at the solid surface boundary. Boundary conditions for each reacting species are individually computed from species mass balance at the surface, where species diffusion balances catalytic production for a non-ablating wall and a self-consistent diffusion model enforces total mixture diffusion flux conservation. The non-catalytic wall boundary condition enforces zero catalytic production for each species, which implies that diffusion flux for each will be zero. The "super-catalytic" boundary condition sets a mixture composition explicitly at the surface that coincides with the lowest energy composition of the gas without regard for reaction kinetics or reactant availability. The super-catalytic boundary condition enforces a non-physical set of catalytic production rates at the surface, but does provide an upper limit on energy release at the surface and thus a conservative estimate of heat transfer rate. The specified reaction efficiency (SRE) model enforces a user-specified efficiency for homogeneous catalytic reactions based on the fraction of reactant species that reach the surface for which a recombination event occurs. The reaction efficiency (or reactant loss efficiency), γ, may be specified as constant or as a function of temperature resulting from empirical curve-fit of experimental data. Very recently, a generalized, physics-based finite rate surface chemistry (FRSC) model[27-28] has been implemented in the DPLR code that allows for an arbitrary number of physical reaction forms such as Eley-Rideal and Langmuir-Hinshelwood recombination events to be specified. Gas phase reactants interact with adsorbed surface and bulk (thermal protection system) species through physical processes that can be used to model both catalytic and ablation events. However, the FRSC model requires specification of a large number of physical parameters that must be obtained for each environment and has not yet gained widespread use.

For carbon dioxide systems, two primary mechanisms occur for surface reaction. At reentry conditions, the shock layer consists primarily of CO and O, which may react at the surface. Competition for available oxygen atoms occurs between the two following reactions:

$$O + O \rightarrow O_2 \tag{1}$$

$$CO + O \rightarrow CO_2 \tag{2}$$

Limited experimental evidence suggests that Eq. (1) should prevail[29]. However, since the objective is to provide bounding comparisons to the data, we have provided two solutions in addition to the non-catalytic and super-catalytic bounding solutions, where we first assume that Eq. (1) reacts with complete efficiency (γ=1.0) and then Eq. (2) reacts with complete efficiency (γ=1.0), neglecting the other reaction in each case. There is no direct experimental evidence of the process efficiencies in the LENS-XX environment yet, but these boundary conditions provide more physical limiting cases than the super-catalytic model since reactant competition is at least included.

A detailed numerical uncertainty study has been previously shown for reacting air cases with this same model[5]. For these reacting laminar flows, uncertainty in the physics models of the gas phase thermochemistry and the surface catalytic reactions dominate the accuracy of the numerical solutions. For well-tailored grids, the solutions converge to approximately machine zero accuracy and dependency on the grid was found to amount to an error in heat flux of at most 3%, which is well within the noise of the comparisons. This uncertainty study is not repeated here since the results with CO_2 will be similar.

D. Experimental Measurement Techniques

Accurate heat transfer measurements are made on cold-wall (300 K) stainless-steel models using several types of instruments. The primary gage is the platinum thin-film gage, which is a platinum resistance temperature detector (RTD) painted on a substrate of Pyrex. These gages can be isolated on a Pyrex island of between 1-mm and 3-mm in diameter on an otherwise metallic surface or painted along a continuous Pyrex strip to provide continuity of surface properties. A very thin layer of Magnesium Fluoride is deposited on the surface of the gage before the initial installation. Each gage is individually calibrated across the expected temperature range. The second type of instrument is the chromel-constantan coaxial thermocouple. The thermocouple junction is formed by depositing a layer of chromium across the surface of the gage, which is the material exposed on the surface upon installation.

In both cases, the short runtime of the shock and expansion tunnel facilities allows the heat transfer to be reduced from measured surface temperature history using one-dimensional conduction on a semi-infinite solid. The short duration of flow in the facilities limits the temperature rise that will occur during the runtime. Ending temperature varies with conditions, but, for the types of conditions considered here, temperature rises for the thermocouples will be on the order of 10 K and for the thin-films on the order of 100 K over the approximately 1 ms time period.

Standard uncertainties in the heat transfer sensors are ±5% for thin-film gages and ±8% for coaxial thermocouple gages (using conduction properties specified by the manufacturer). In this work, we report error bars on each individual sensor using the standard deviation of that sensor during the averaging window, which incorporates sensor uncertainty as well as facility, freestream, and shock layer fluctuation. In most cases, the standard deviation is similar to or just slightly exceeds the quoted sensor uncertainty, providing some notional indications of the flow quality.

E. Total Enthalpy Conventions Associated with High Enthalpy Carbon Dioxide Testing

A common convention in use in the hypersonics community is to assign the formation (chemical) enthalpy of diatomic gaseous oxygen and solid carbon to be zero at 0 K and derive formation enthalpy values for each reacting species from these and other references. Doing so results in a formation enthalpy for carbon dioxide, CO_2, of -8.93 MJ/kg that must be included in reacting flow calculations. The formation enthalpies of CO_2 and all other species that are considered in the system are correctly incorporated into both the CHEETAh calculations of freestream conditions as well as the DPLR simulations of the shock layer, but a consequence of this inclusion is that the absolute total enthalpy of the system state (typically pure CO_2 in the freestream) has a large negative heat of formation component which results in negative or small, positive values that are very much smaller than the kinetic energy term ($^1/_2\, U_\infty^2$) one usually expects total enthalpy to closely match in hypersonic flows. This problem does not occur with air flows since the assigned heats of formation of both O_2 and N_2 species are zero at 0 K.

To make the total enthalpy of each condition more intuitive, we employ a particular convention here by taking the difference between the total enthalpy of the freestream test gas (sensible plus chemical plus kinetic) and the total enthalpy of the initial state of the test gas in the facility (sensible plus chemical, where kinetic is zero) and designate this quantity Δh_0. Thus, in the expansion tunnel, this parameter is defined as in Eq. (3), or the total enthalpy of State 5 minus the total enthalpy of State 1 as defined in Fig. 2.

$$\Delta h_0 \equiv h_0^{[State\,5]} - h_0^{[State\,1]} \tag{3}$$

The definition in the reflected shock tunnel environment discussed in the next section is similar, where Δh_0 is defined as the total enthalpy in the reservoir minus the total enthalpy of the initial driven state.

In either case, the initial State 1 or driven gas state of carbon dioxide is the absolute enthalpy of the gas at room temperature (293 K), or approximately -8.72 MJ/kg. As defined, Δh_0 is equal to the amount of enthalpy added to the test gas by the unsteady gasdynamic process in each facility.

III. Review of Measurements from LENS-I Reflected Shock Tunnel

A number of recent studies which made measurements in high enthalpy carbon dioxide have been performed in reflected shock tunnel environments. A two-phase study was performed with 70^O sphere-cone models at CUBRC in the LENS-I shock tunnel, which reported a number of unexplained results[30-32]. The measured heat transfer data, when compared with CFD solutions, showed a tendency to best agree with predictions using the super-catalytic boundary condition as defined here (assuming complete recombination to carbon dioxide on the surface). This observation was also independently made in the Caltech T5 shock tunnel facility[33]. For some conditions at the lowest Reynolds numbers tested in LENS-I, the experimental data showed a bizarre behavior where the heating nearest the stagnation point was observed to be significantly less than super-catalytic and the heating on the cone frustum was observed to be approximately super-catalytic, as shown in Fig. 3(a). Secondly, in LENS-I, gross under-prediction of the bow shock stand-off and curvature was observed, exacerbated at low Reynolds numbers as demonstrated in Fig. 3(b). Finally, in Fig. 3(c) a number of runs at angle of attack showed heat flux augmentation that occurred on the windward side of the heat shield that could not be readily attributed to transitional or turbulent flow by considering any of the transition metrics employed by the program.

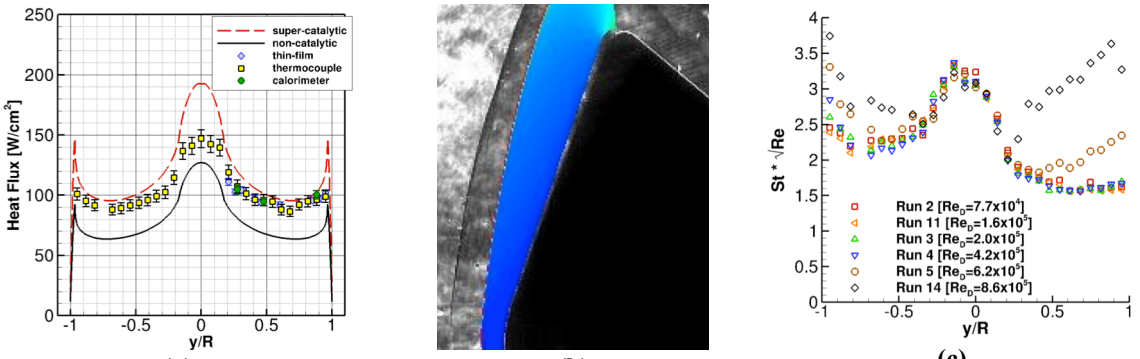

(a) (b) (c)

Figure 3. Comparison between Measured and Predicted Shock Stand-off and Surface Heat Transfer in the LENS-I Reflected Shock Tunnel Test with High Enthalpy Carbon Dioxide

An analysis performed by MacLean and Holden[34] showed that, for a typical run condition in the LENS-I study at an effective flow enthalpy of 5 MJ/kg, the distribution of energy in the high temperature, stagnant reservoir of the reflected shock tunnel holds 57% of the total enthalpy in vibrational and chemical storage. These potential non-equilibrium storage mechanisms were assessed to determine the amount of chemical or vibrational freezing during the nozzle expansion process that would be required to match the significantly larger shock stand-off distance observed in the experiment (Fig. 3(b)). Assigning arbitrary percentages of the total enthalpy to non-equilibrium modes in the freestream alters the stand-off distance of the prediction, and, through trial and error, shows that 42% of the total enthalpy in non-equilibrium in the freestream matches the measured shock standoff distance as shown in Fig. 4(a). In the study, both non-equilibrium vibration and non-equilibrium chemistry (dissociation) were considered, but the effect of non-equilibrium in the freestream on shock stand-off distance is related only to the rate at which the non-equilibrium relaxes behind the shock and not on the physical storage mechanism. In other words, non-equilibrium chemistry in the freestream appears to have less of an effect because the chemical rates employed are slower than the vibration-translation exchange rates in the study. Interestingly, the heat flux predictions using this large percentage of freestream non-equilibrium reduces the predicted heat transfer near the stagnation point and brings the super-catalytic wall solution more closely in line with the data without significantly changing the comparison on the frustum in Fig. 4(b).

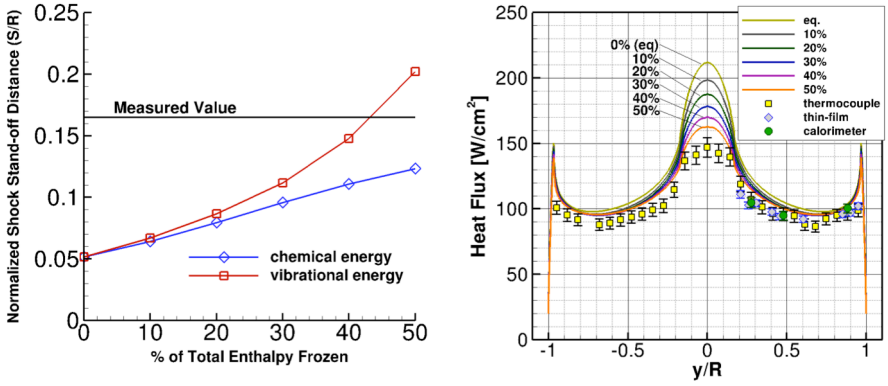

(a) (b)

Figure 4. Effect of Freestream Non-equilibrium Energy on Shock Stand-off and Surface Heat Transfer for Run 8 in the LENS-I Reflected Shock Tunnel Test with High Enthalpy Carbon Dioxide

Although this analysis does demonstrate that agreement with the measured shock stand-off distance is possible, it does not identify a detailed physical mechanism(s) by which the expanding flow transfers such a large quantity of energy to non-equilibrium modes. However, the contrived freestream condition is at least consistent with the experimental observations and is consistent with the observation that the shock stand-off discrepancy decreases steadily with increasing Reynolds number as shown in Fig. 5, which shows the comparison of the predicted and measured bow shock profiles for a series of runs at the same enthalpy (Δh_0 ~ 5 MJ/kg) and angle of attack (11^O) where the facility total pressure and, hence, freestream density is increased. The comparisons show that the discrepancy between the experiment and CFD reduces as the density increases and more molecular collisions occur in the nozzle expansion. However, even at the highest densities that were tested, the agreement is still not good. This analysis along with the (seemingly fortuitous) agreement with the super-catalytic prediction of heat transfer observed in the reflected shock tunnel facilities is troubling and suggests that the conditions of the test are not well

understood. This conclusion has also been shown by Hollis and Prabhu[4], who demonstrated poor agreement between ground test experiment and CFD with every low Reynolds number, laminar dataset that they could find obtained in high-enthalpy carbon dioxide ground test environments.

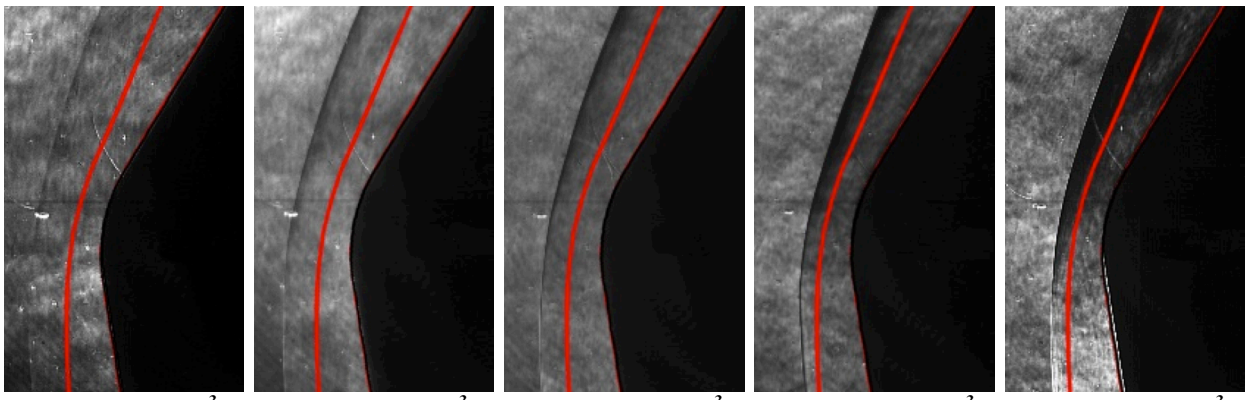

(a) ρ = 3.0 g/cm^3 S/S$_{CFD}$ = 2.71 | **(b) ρ = 8.4 g/cm^3 S/S$_{CFD}$ = 2.47** | **(c) ρ = 17.6 g/cm^3 S/S$_{CFD}$ = 2.12** | **(d) ρ = 26.2 g/cm^3 S/S$_{CFD}$ = 1.71** | **(e) ρ = 36.3 g/cm^3 S/S$_{CFD}$ = 1.70**

Figure 5. Comparison between Measured and Predicted Shock Stand-off for a Series of Conditions in the Reflected Shock Tunnel Environment with Varying Freestream Density (Freestream Density and Ratio of Experimental to Computational Standoff at Nosetip Listed for Each)

IV. New Measurements Made in the LENS-XX Expansion Tunnel

An exploratory series of experiments was performed in the new LENS-XX facility to assess the viability of a large-scale expansion tunnel facility to provide ground test data in a high-enthalpy reacting carbon dioxide environment without the uncertainties associated with the presumed behavior of the rapidly expanding freestream test gas observed in the reflected shock tunnel environment. To minimize the costs associated with this exploratory effort, tests were performed using an existing 17.8-cm (7-in) diameter spherical capsule model equivalent to a 4.5% scale Apollo or a 3.5% scale Orion/MPCV smooth-body heat shield[5]. Although NASA has never used the spherical capsule heat shield geometry for Mars entry, the goal of this effort was to acquire experimental data with which to make comparisons against CFD simulations. The necessary dimensions of the model used are shown in Fig. 6(a). Only the heat shield of the capsule vehicle was replicated in this test to a station just downstream of the heat shield shoulders. The backshell components of the model were not instrumented, nor representative of any flyable configuration. The model instrumentation consisted of a ray of 26 coaxial thermocouples and 13 thin-film heat flux gages along the centerplane of the model shown in Fig. 6(b). Additionally, four flush mounted piezoelectric pressure gages were installed on the heat shield just off center at a lateral station located 1.9-cm from the centerplane as a check of freestream conditions and model angularity. At the angles of attack studied in this test, the windward pressure sensor measures a pressure level very close to the facility Pitot pressure. Schlieren images were also obtained for each run in this test series, with the high-speed camera synchronized to a copper-vapor laser as the light source. The frame shown in this publication corresponds closely with the middle of the averaging window for the surface data. The capsule model installed in the facility is shown in Fig. 6(c). In addition to the primary model, there are several secondary facility diagnostics also running in the test section just below the spherical capsule model.

Table 1. Freestream Conditions for Spherical Capsule CO_2 Study

Run #	*Δh_0 (MJ/kg)*	*U (km/s)*	*ρ (g/m^3)*	*P (Pa)*	*T (K)*	*AOA (^{O})*
9	7.61	3.88	1.829	133	385	18
10	11.69	4.78	0.797	84	555	18
11	15.30	5.45	0.294	41	743	18
12	8.26	4.04	0.636	48	397	18
14	23.54	6.42	0.988	408	2056	20
	c_{CO2} = 0.878224 | c_{CO} = 0.077506 | c_{O2} = 0.042819 | c_O = 0.001451					
15	15.54	5.44	.520	288	1006	20

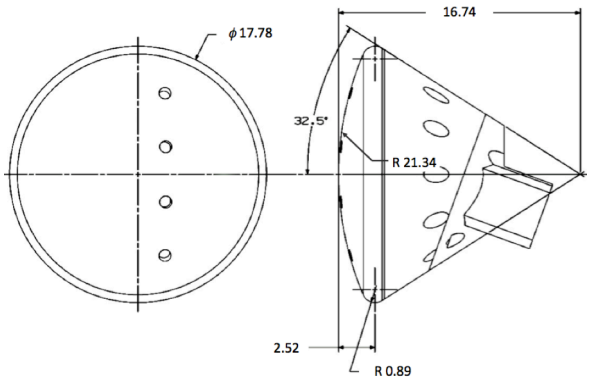

(a) dimensions in [cm]

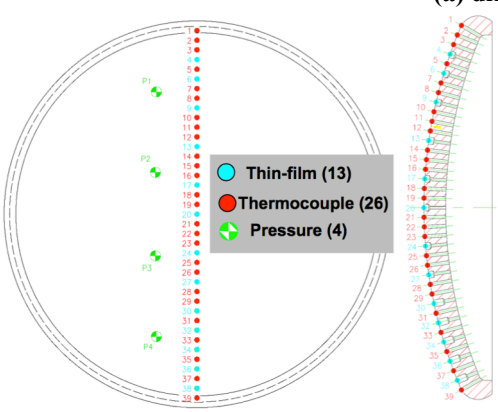

(b)

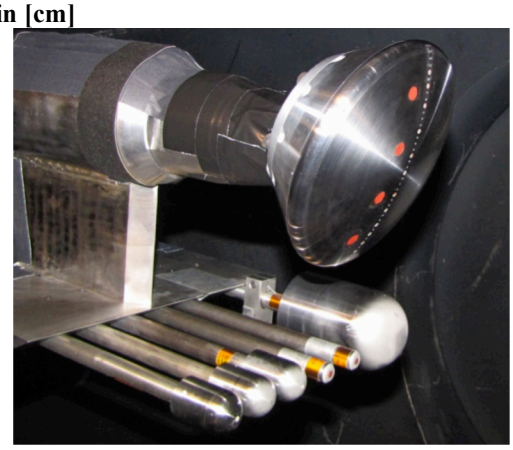

(c)

Figure 6. Model Dimensions, Instrumentation, and Installation into the LENS-XX Facility

The freestream test conditions for these tests are given in Table 1. These tests covered a range of total enthalpy from 7.6 to 23.5 MJ/kg. Six runs are listed in the table whose results will be discussed here. These tests were conducted in two phases, with Runs 09 – 12 performed in the first phase and Runs 14 and 15 performed in the second phase along with some calibration and diagnostic runs not discussed here. The angle of attack of the model was changed slightly between the two test entries. Table 1 also shows that the highest enthalpy condition, Run 14, has a freestream that is slightly dissociated because of the relatively high freestream temperature necessary at this extreme enthalpy. We observe that, although there is some freestream dissociation, the test gas has not gone through the same rapid expansion from stagnation that occurs in the reflected shock tunnels.

The chemical mass fraction profiles predicted by the CFD using the nominal chemical model for each of these test cases along the stagnation line are shown in Fig. 7 to provide some feeling for the relative importance of certain chemical processes. In all cases, significant carbon monoxide (CO) forms behind the bow shock and the relaxation of the translational temperature shown in each figure demonstrates that the flow is in a state of chemical non-equilibrium for all cases. In Run 14, the enthalpy is high enough to involve carbon atom formation (at least predicted by CFD), though it is negligible in the other cases.

The comparison between the predicted bow shock contours, scaled to highlight the shape of the bow shock, and the measured Schlieren image for each run is shown in Figs. 8 – 13. Each figure shows a tare image taken just before the flow arrives for each run in (a), followed by an image taken within the window over which the surface data is averaged in (b), and an overlay of the CFD solution onto the flow image in (c). The CFD solution was constructed as a computational Schlieren by computing the magnitude of the density gradient and setting the minimum scale such that only the bow shock and the boundary layer are visible. The CFD contour image has been lined up on the experimental image for each case using a tare image taken before each run using a digital photography manipulation program. The tare image is easier to work with because the density gradients near the surface with flow on and the reflection off the model surface can obscure the exact location of the surface. As each CFD solution has been rotated to fit the surface of the tare image, any rotational misalignment the camera due to setting up the camera tripod next to the facility is also accounted for.

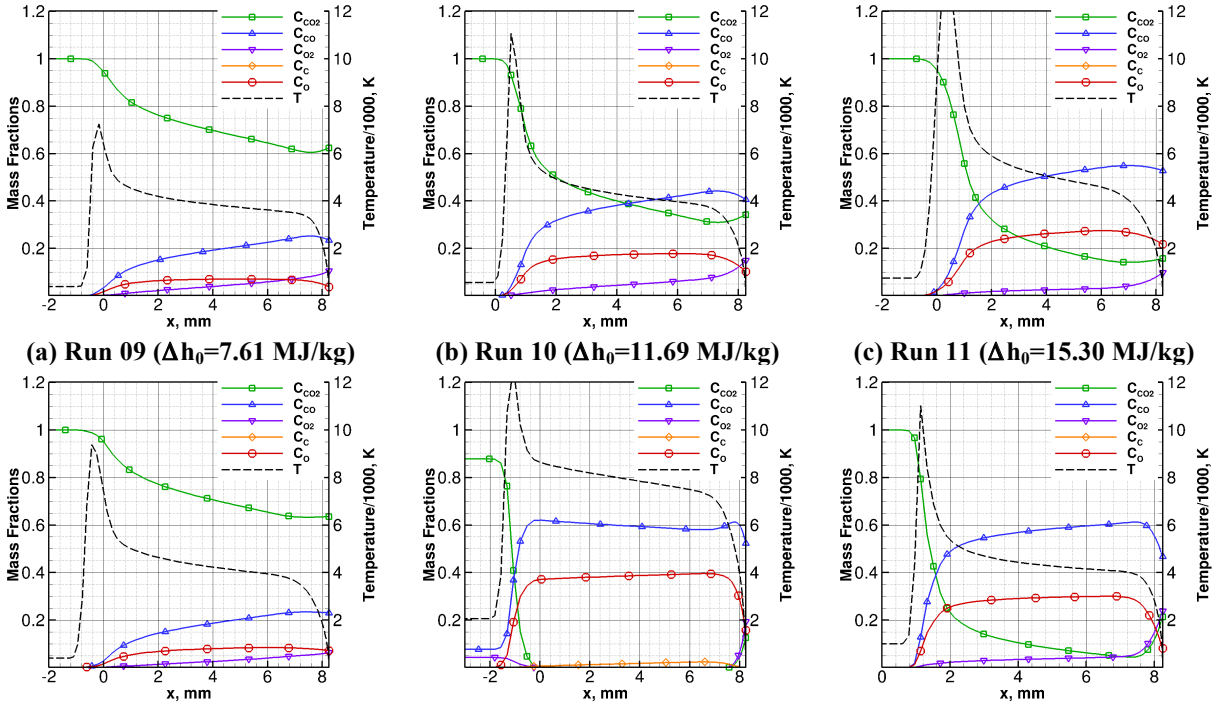

(a) Run 09 (Δh_0=7.61 MJ/kg) **(b) Run 10 (Δh_0=11.69 MJ/kg)** **(c) Run 11 (Δh_0=15.30 MJ/kg)**

(d) Run 12 (Δh_0=8.26 MJ/kg) **(e) Run 14 (Δh_0=23.54 MJ/kg)** **(f) Run 15 (Δh_0=15.54 MJ/kg)**

Figure 7. Chemical Mass Fraction Profiles along Stagnation Line for All Runs

Good agreement is obtained for all run conditions, even the high enthalpy Run 14 where the freestream flow is slightly dissociated. This agreement may be contrasted with the gross misalignment between prediction and experiment observed in the reflected shock tunnel experiments discussed in the previous section (Figs. 3(b) and 5). This result implies that even a small amount of residual dissociation in the freestream of the expansion tunnel facility can be tolerated since the test gas does not undergo expansion from stagnant conditions.

The comparison between CFD and experiment with surface pressure is shown for all runs in Fig. 14. In general, the agreement between the CFD and the measurements is very good. The rightmost pressure sensor for Run 14 in Fig. 14(e) is slightly out of bounds from the prediction. Since this is the highest enthalpy run, it is unclear if this is significant or just an anomalous reading. The pressure sensor nearest the stagnation point malfunctioned during Run 15 and is not available for comparison in Fig. 14(f), but the other three sensors show good agreement.

Finally, the measured heat transfer distributions for each run are compared to several CFD solutions in Fig. 15. For each run, available thin-film sensors are shown with a diamond symbol and coaxial thermocouple sensors are shown with square symbols. A number of things can be observed in this data. First, the coaxial thermocouple and the thin-film sensors generally measure consistent levels of heat transfer. Also, in general, the thin-film sensors are observed to have smaller standard deviations in the signals than the coaxial thermocouples, which is consistent with how they perform in the reflected shock tunnels facilities. However, standard deviation varies from sensor to sensor.

Most importantly, the data lies well within the bounds established by the non-catalytic and super-catalytic CFD solutions. This behavior is in contrast with the results found in earlier studies in other types of facilities and is much more consistent with physical intuition. In general, it is also observed that the solution corresponding to the $CO+O \rightarrow CO_2$ reaction over-predicts the data, implying that this process does not occur with appreciable efficiency. Across all runs, the solution corresponding to $O+O \rightarrow O_2$ best reproduces the data, although it does somewhat under-predict the data for Run 10 in Fig. 15(b) and for Run 15 in Fig. 15(f). However, we emphasize again that all of these comparisons rely on a particular set of transport models, chemical dissociation rates, vibrational relaxation rates, vibration-dissociation coupling models, etc. that are largely un-validated at these conditions. Improvements in any of these models may change the interpretation of the surface heating data. We emphasize again that the objective of this test has not been to validate any of the particular CFD models employed in this work, but to provide a quality dataset for the validation of future computational models of gaseous chemistry and fluid transport at conditions relevant to Martian entry.

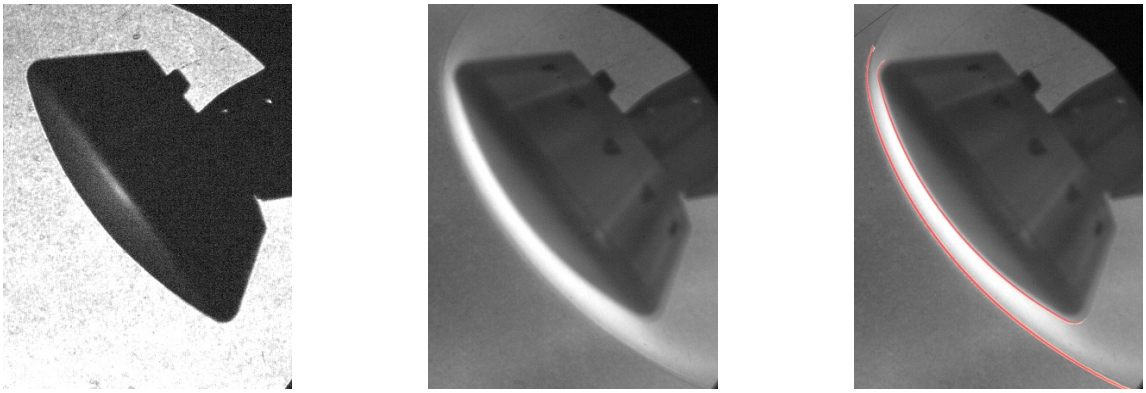

(a) tare image **(b) flow image** **(c) CFD overlay**

Figure 8. Measured Schlieren Still Frame Compared to CFD Mach Number Contours for Run 09

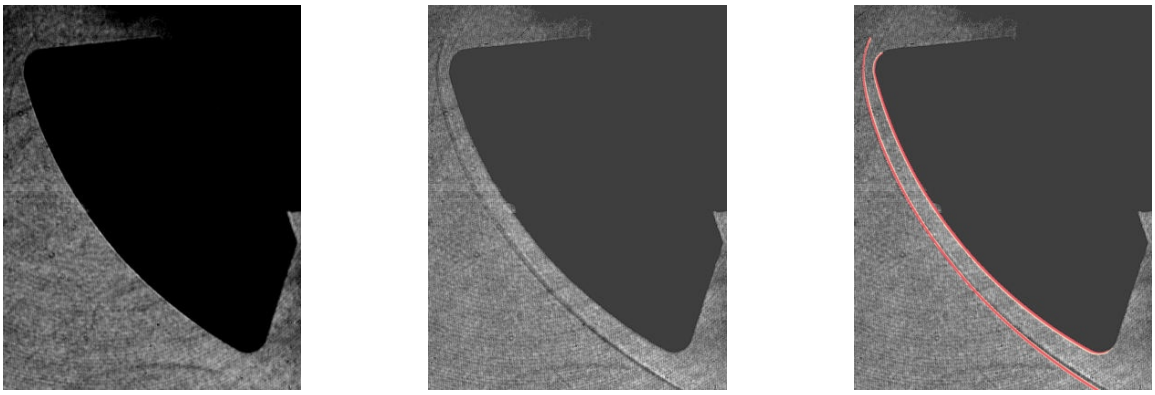

(a) tare image **(b) flow image** **(c) CFD overlay**

Figure 9. Measured Schlieren Still Frame Compared to CFD Mach Number Contours for Run 10

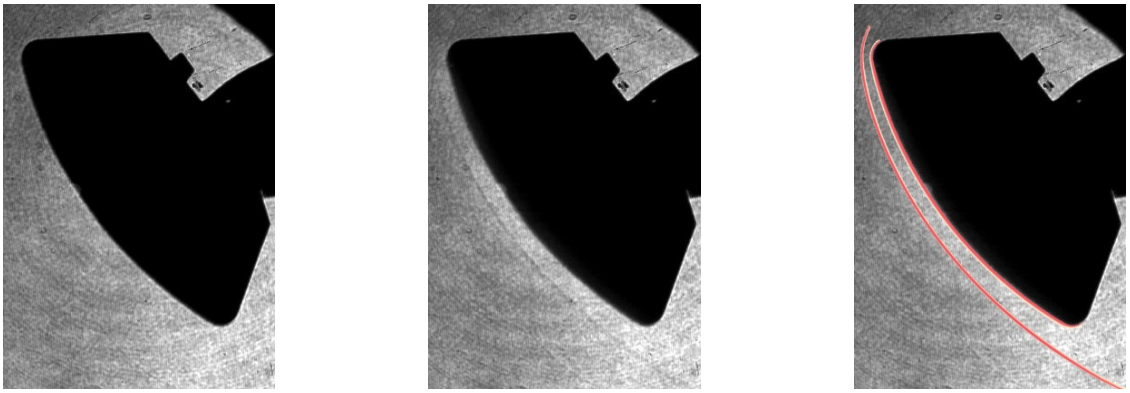

(a) tare image **(b) flow image** **(c) CFD overlay**

Figure 10. Measured Schlieren Still Frame Compared to CFD Mach Number Contours for Run 11

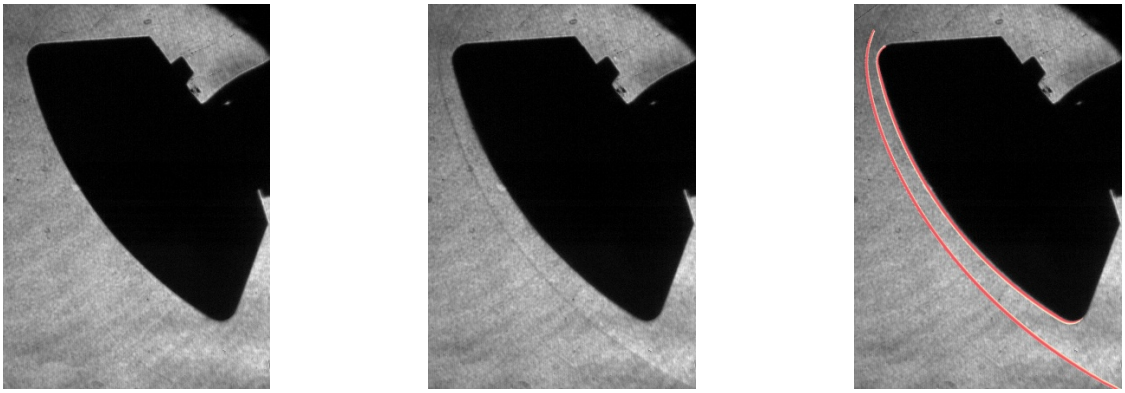

(a) tare image **(b) flow image** **(c) CFD overlay**

Figure 11. Measured Schlieren Still Frame Compared to CFD Mach Number Contours for Run 12

(a) tare image **(b) flow image** **(c) CFD overlay**

Figure 12. Measured Schlieren Still Frame Compared to CFD Mach Number Contours for Run 14

(a) tare image **(b) flow image** **(c) CFD overlay**

Figure 13. Measured Schlieren Still Frame Compared to CFD Mach Number Contours for Run 15

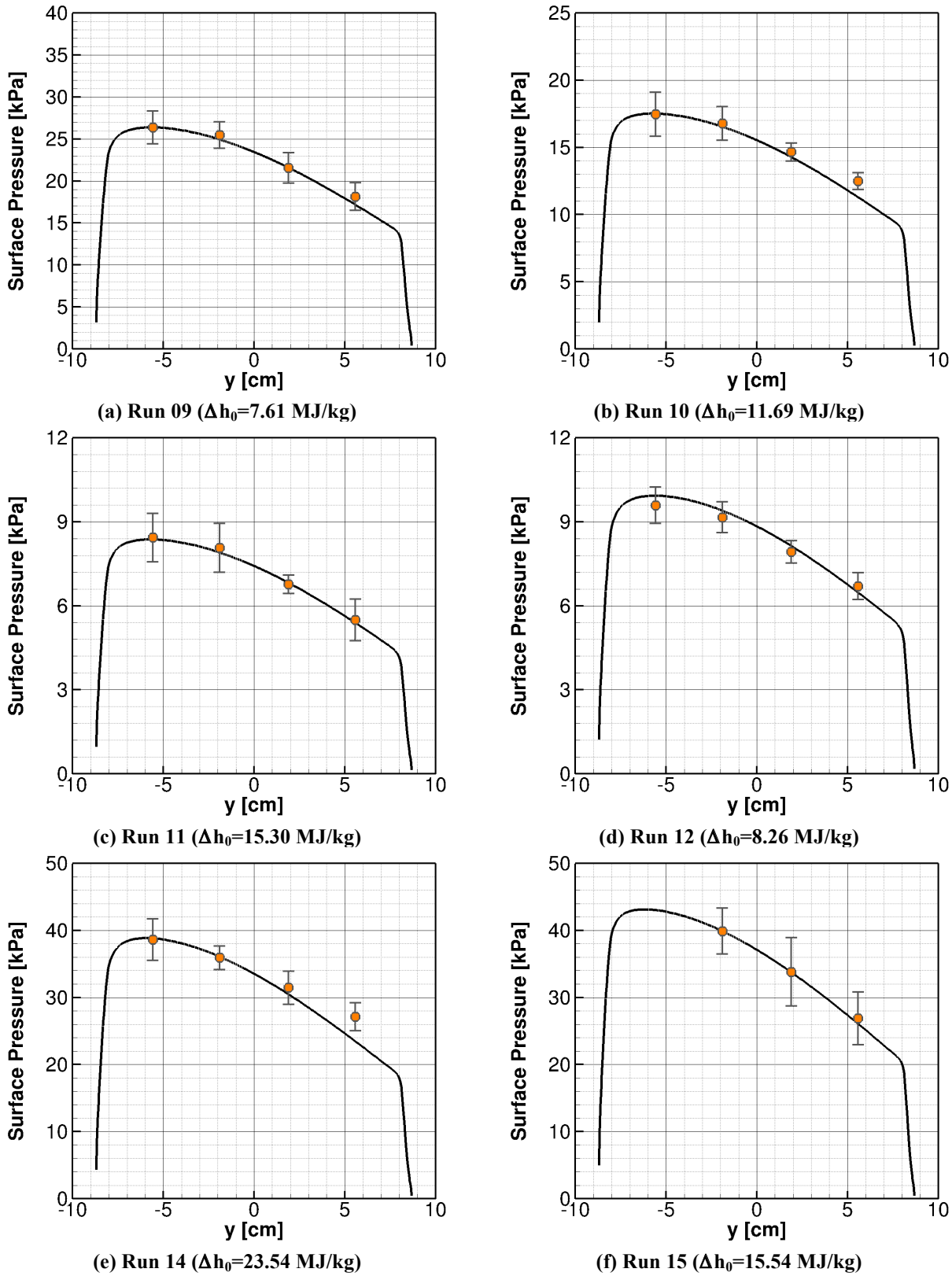

(a) Run 09 (Δh_0=7.61 MJ/kg)

(b) Run 10 (Δh_0=11.69 MJ/kg)

(c) Run 11 (Δh_0=15.30 MJ/kg)

(d) Run 12 (Δh_0=8.26 MJ/kg)

(e) Run 14 (Δh_0=23.54 MJ/kg)

(f) Run 15 (Δh_0=15.54 MJ/kg)

Figure 14. Measured and Predicted Surface Pressure Distributions for All Runs

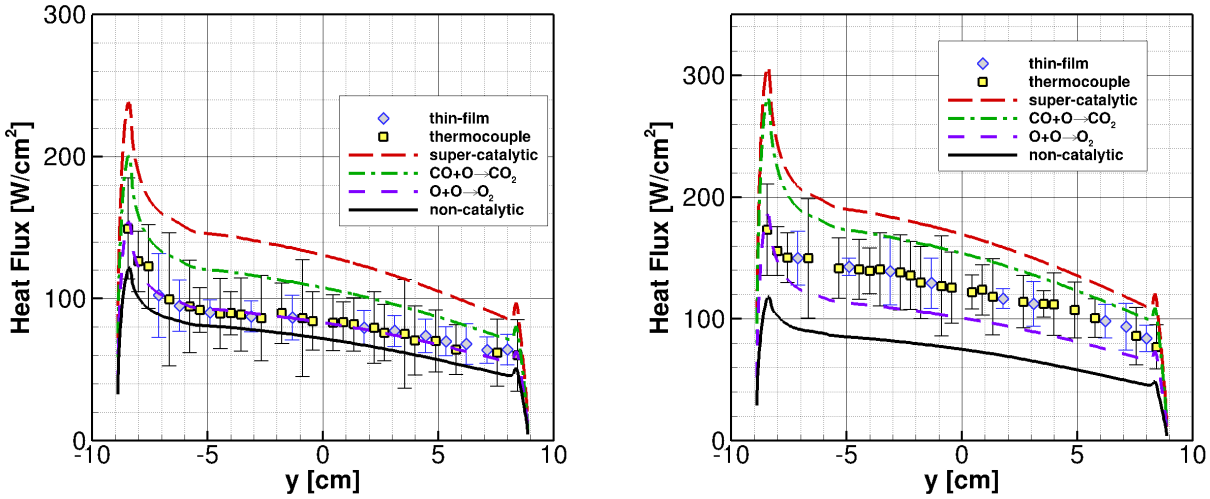

(a) Run 09 (Δh_0=7.61 MJ/kg)

(b) Run 10 (Δh_0=11.69 MJ/kg)

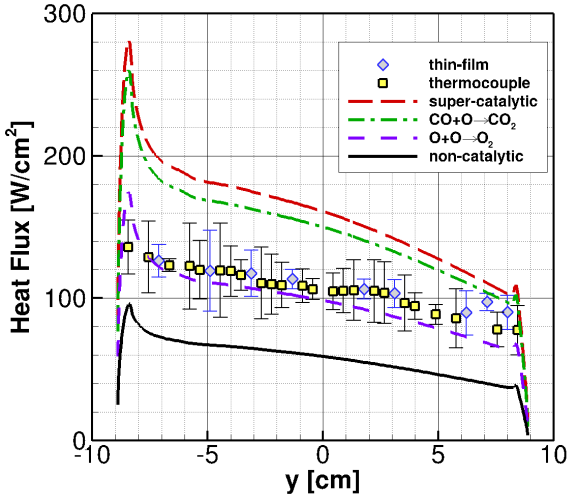

(c) Run 11 (Δh_0=15.30 MJ/kg)

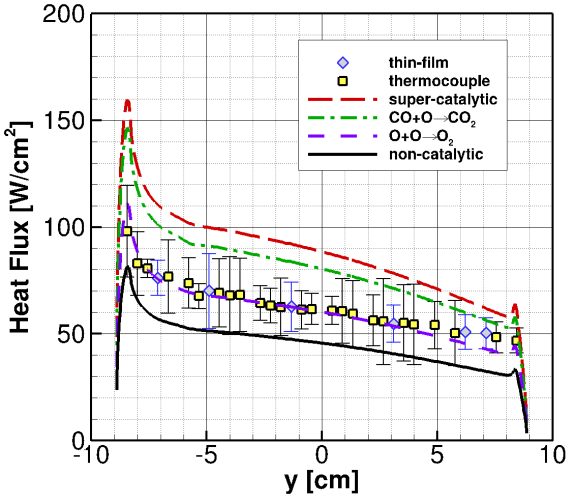

(d) Run 12 (Δh_0=8.26 MJ/kg)

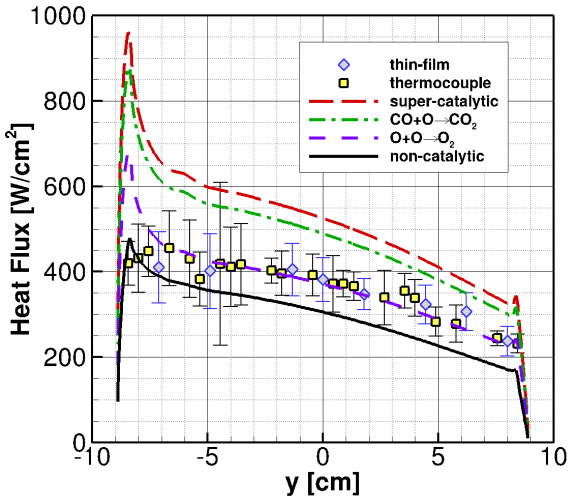

(e) Run 14 (Δh_0=23.54 MJ/kg)

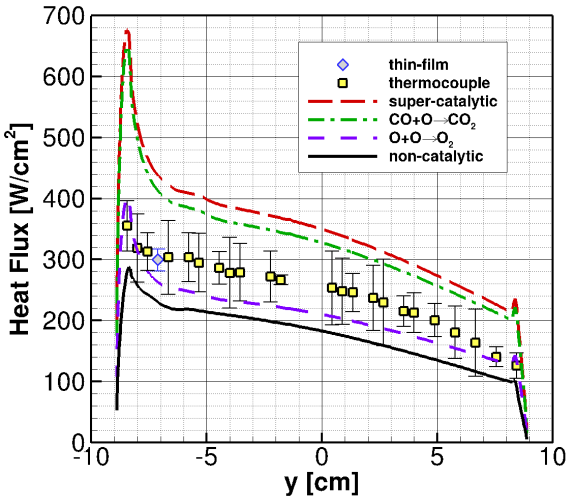

(f) Run 15 (Δh_0=15.54 MJ/kg)

Figure 15. Measured and Predicted Surface Heat Flux Distributions for All Runs

V. Conclusions

The LENS-XX expansion tunnel facility has been used for a preliminary experimental study of laminar blunt body heating on a spherical capsule shape at freestream velocities of 3.9 to 6.4 km/s, or 7.6 to 23.5 MJ/kg of total enthalpy increase. These experimental measurements have been made at the range of flight velocities relevant to entry into the Martian atmosphere using pure carbon dioxide as a test gas (neglecting the small percentage of nitrogen present on Mars). In previous studies in reflected shock tunnels, a number of anomalies have been observed in the test data. Most prominently, measured shock stand-off was observed to be in excess of a factor of two larger than prediction for low Reynolds number laminar flow conditions in the LENS-I facility. Additionally, a number of facilities have observed heat transfer levels consistent with complete recombination to carbon dioxide at the surface for low Reynolds number, laminar conditions. In this exploratory test series, shock shape and stand-off distance has been observed to agree well with prediction for all conditions; no evidence of the massive shock stand-off discrepancy observed in the LENS-I test series can be seen.

Additionally, using the established baseline chemical relaxation, vibrational relaxation, and transport property models for CFD, measured heat transfer distributions show levels significantly less than the super-catalytic and the $CO + O \rightarrow CO_2$ diffusion limited reaction solutions, suggesting that formation of carbon dioxide at the surface is not prevalent. This result is a major departure from the earlier observations in the LENS-I facility and other reflected shock tunnel tests. However, agreement between the experimental measurements is a function of both gas phase modeling (chemistry rates, vibrational relaxation rates, diffusion coefficients, etc.) and surface catalytic reactions. The goal of an experimental study such as this is to provide validation data for new and/or improved physical models of the gaseous kinetic behavior of the carbon dioxide system. This preliminary study of reacting carbon dioxide at total enthalpy levels relevant to EDL on Mars has been highly successful in meeting this objective. However, decoupling the gaseous kinetic and the catalytic behavior of the gas in the expansion tunnel environment remains a significant issue that must be considered in future studies.

Acknowledgments

This work was sponsored by the NASA Fundamental Aeronautics Program with Dr. Deepak Bose acting as program manager.

References

[1]Wright, M.; Tang, C.; Edquist, K.; Hollis, B.; Krasa, P.; and Campbell, C. "A Review of Aerothermal Modeling for Mars Entry Missions," AIAA Paper 2010 – 0443, 48TH AIAA Aerospace Sciences Meeting & Exhibit, Orlando, FL: 4-7 January 2010.

[2]Cianciolo, A.; Zang, T.; Sostaric, R.; and Mcguire, M.K. "Overview of the NASA Entry, Descent and Landing Systems Analysis Exploration Feed-Forward Study," Session 6B, Proceedings of the 8TH International Planetary Probe Workshop, Portsmith, VA: 6 – 10 June 2011.

[3]Gazarik, M., et. al, "Overview of the MEDLI Project," IEEE Paper 2008-1510, IEEE Aerospace Conference, Big Sky, MT, March 2008.

[4]Hollis, B. and Prabhu, D. "Assessment of Laminar, Convective Aeroheating Prediction Uncertainties for Mars Entry Vehicles," AIAA Paper 2011–3144. 42ND Thermophysics Conference, Honolulu, HI: 27 – 30 June 2011.

[5]Dufrene, A.; MacLean, M.; Wadhams, T.; and Holden, M. "High Enthalpy Studies of Capsule Heating in an Expansion Tunnel Facility." AIAA Paper 2012–2998. 43RD AIAA Thermophysics Conference, New Orleans, LA: 25–28 June 2012.

[6]Holden, M.S. and Parker, R.P. "LENS Hypervelocity Tunnels and Application to Vehicle Testing at Duplicated Flight Conditions," Chp 4 of *Advanced Hypersonic Test Facilities*. Lu, F.K. and Marren, D.E. Eds. AIAA Progress in Astronautics and Aeronautics Series: Vol 198. Chapter 4. Reston, VA: American Institute of Aeronautics and Astronautics, 2002.

[7]Holden, M.S.; Wadhams, T.P.; and Candler, G.V. "Experimental Studies in the LENS Shock Tunnel and Expansion Tunnel to Examine Real-Gas Effects in Hypervelocity Flows". AIAA Paper 2004-0916. January 2004.

[8]Dufrene, A.; Sharma, M.; and Austin, J.M. "Design and Characterization of a Hypervelocity Expansion Tube Facility," AIAA Paper 2007–1327. 45TH Aerospace Sciences Meeting & Exhibit. Reno, NV: 8-11 January 2007.

[9]Dufrene, A.; MacLean, M.; Parker, R.; Wadhams, T.; and Holden, M. "Characterization of the New LENS Expansion Tunnel Facility." AIAA Paper 2010-1564. 48TH AIAA Aerospace Sciences Meeting & Exhibit, Orlando, FL: 4-7 January 2010.

[10]Dufrene, A.; MacLean, M.; and Holden, M. "Experimental Characterization of the LENS Expansion Tunnel Facility Including Blunt Body Surface Heating." AIAA Paper 2011-0626. 49TH AIAA Aerospace Sciences Meeting, Orlando, FL: 4-7 January 2011.

[11]MacLean, M.; Dufrene, A.; Wadhams, T.; and Holden, M. "Numerical and Experimental Characterization of High Enthalpy Flow in an Expansion Tunnel Facility." AIAA Paper 2010-1562. 48TH AIAA Aerospace Sciences Meeting & Exhibit, Orlando, FL: 4-7 January 2010.

[12]Parker, R.; Dufrene, A.; MacLean, M.; Holden, M.; DesJardin, P.; and Weisberger, J. "Emission Measurements from High Enthalpy Flow on a Cylinder in the LENS XX Hypervelocity Expansion Tunnel," Accepted for 2013 Aerospace Sciences Meeting in Dallas, TX.

[13]Wright, M.J.; Bose, D.; and Candler, G.V. "A Data Parallel Line Relaxation Method for the Navier-Stokes Equations". *AIAA Journal*. Vol 36, no 9. Pgs 1603 – 1609. Sept 1998.

[14]MacCormack, R.W. and Candler, G.V. "The Solution of the Navier-Stokes Equations Using Gauss-Seidel Line Relaxation". *Computers and Fluids*. Vol 17, No 1. Pgs 135 – 150. 1989.

[15]Palmer, G.E. and Wright, M.J. "A Comparison of Methods to Compute High Temperature Gas Viscosity". *Journal of Thermophysics and Heat Transfer*. Vol 17, no 2. Pgs 232 – 239. 2003.

[16]Palmer, G.E. and Wright, M.J. "A Comparison of Methods to Compute High Temperature Gas Thermal Conductivity". AIAA Paper 2003-3913. Jun 2003.

[17]Gupta, R.; Yos, J.; Thompson, R.; and Lee, K. "A Review of Reaction Rates and Thermodynamic and Transport Properties for an 11-Species Air Model for Chemical and Thermal Nonequilibrium Calculations to 30000 K". NASA RP-1232. August 1990.

[18]Wright, M.J.; Bose, D.; Palmer, G.E.; and Levin, E. "Recommended Collision Integrals for Transport Property Computations, Part 1: Air Species," *AIAA Journal*, Vol 43, No 12, Pgs 2558 – 2564. December 2005.

[19]Wright, M.; Hwang, H.; and Schwenke, D. "Recommended Collision Integrals for Transport Property Computations Part 2: Mars and Venus Entries," *AIAA Journal*, Vol 45, No 1, January 2007, Pgs 281 – 288.

[20]Ramshaw, J.D. "Self-consistent Effective Binary Diffusion in Multicomponent Gas Mixtures". *Journal of Non-Equilibrium Thermodynamics*. Vol 15, no 3. Pgs 295 – 300. 1990.

[21]Park, C.; Howe, J.T.; Jaffe, R.J.; and Candler, G.V. "Review of Chemical-Kinetic Problems of Future NASA Missions II: Mars Entries". *Journal of Thermophysics and Heat Transfer*. Vol 8, no 1. Pgs 9 – 23. 1994.

[22]Candler, G.V. "Chemistry of External Flows". *Aerothermochemistry for Hypersonic Technology*: Von Karman Institute for Fluid Dynamics Lecture Series. VKI LS 1995-04.

[23]Landau, L. and Teller, E. "Theory of Sound Dispersion". *Physikalische Zeitschrift der Sowjetunion*. Vol 10, no 34. 1936.

[24]Millikan, R. and White, D. "Systematics of Vibrational Relaxation". *Journal of Chemical Physics*. Vol 39, no 12. Pgs 3209 – 3213. 1963.

[25]Camac, M. "CO_2 Relaxation Processes in Shock Waves". *Fundamental Phenomena in Hypersonic Flow*. J.G. Hall Ed. Cornell University Press. Pgs 195 – 215, 1964.

[26]Park, Chul. "Assessment of Two-temperature Kinetic Model for Ionizing Air". AIAA Paper 87-1574. AIAA 22ND Thermophysics Conference. Honolulu, HI: 8-10 June 1987.

[27]Marschall, J. and MacLean, M. "Finite-Rate Surface Chemistry Model, I: Formulation and Reaction System Examples" AIAA Paper 2011–3783. 42ND Thermophysics Conference, Honolulu, HI: 27 – 30 June 2011.

[28]MacLean, M.; Marschall, J.; and Driver, D. "Finite-Rate Surface Chemistry Model, II: Coupling to Viscous Navier-Stokes Code" AIAA Paper 2011–3784. 42ND Thermophysics Conference, Honolulu, HI: 27 – 30 June 2011.

[29]Steinfeld, J I, Francisco, J S, Hase, W L, *Chemical Kinetics and Dynamics*. 2nd Edition, Prentice Hall, 1999.

[30]MacLean, M.; Wadhams, T.; Holden, M.; and Hollis, B. "Investigation of Blunt Bodies with CO2 Test Gas including Catalytic Effects". AIAA Paper 2005–4693. 38TH AIAA Thermophysics Conference, Toronto, CA: 6 – 9 June 2005.

[31]Hollis, B.; Liechty, D.; Wright, M.; Holden, M.; Wadhams, T.; MacLean, M.; and Dyakonov, A. "Transition Onset and Turbulent Heating Measurements for the Mars Science Laboratory Entry Vehicle." AIAA 2005–1437. 43RD AIAA Aerospace Sciences Meeting & Exhibit, Reno, NV, January 2005.

[32]MacLean, M. and Holden, M. "Catalytic effects on Heat transfer Measurements for Aerothermal Studies with CO2." AIAA Paper 2006–0182. 44TH Aerospace Sciences Meeting & Exhibit. Reno, NV: 9-12 January 2006.

[33]Wright, M.; Olejniczak, J.; Brown, J.; Hornung, H.; and Edquist, K. "Computational Modeling of T5 Laminar and Turbulent Heating Data on Blunt Cones, Part 2: Mars Applications," AIAA Paper 2005–0177. 43RD AIAA Aerospace Sciences Meeting and Exhibit, Reno, NV: 10 – 13 January 2005.

[34]MacLean, M. and Holden, M. "Numerical Assessment of Data in Catalytic and Transitional Flows for Martian Entry." AIAA Paper 2006–2946. 9TH AIAA/ASME Joint Thermophysics and Heat Transfer Conference, San Francisco, CA: 5-8 June 2006.